Charge blocking layers in thin-film/amorphous photovoltaics

Osnat Magen and Nir Tessler

Citation: J. Appl. Phys. **120**, 194502 (2016); doi: 10.1063/1.4967921
View online: http://dx.doi.org/10.1063/1.4967921
View Table of Contents: http://aip.scitation.org/toc/jap/120/19
Published by the American Institute of Physics

Charge blocking layers in thin-film/amorphous photovoltaics

Osnat Magen and Nir Tessler[a)]
Zisapel Nano-Electronic Center, Department of Electrical Engineering, Technion - Israel Institute of Technology, Haifa 32000, Israel

(Received 14 October 2016; accepted 3 November 2016; published online 18 November 2016)

The open circuit voltage of solar cells is a critical property which, in many thin film devices, is found to be much lower than the theoretical limit associated with the material's absorption energy gap. A known method for improving the open circuit voltage is that of adding charge blocking layers (a.k.a. charge selective or charge transport layers). However, such interfacial layers are often found to decrease the fill factor or even cause undesired S-shape in J-V curves. In the current work, we revisit the blocking-layer method through detailed device simulations, explain how such layers enable significant Voc increase (even above the built-in voltage), and show that the layers' resistance is responsible for the problematic behavior observed. Having identified the source of reduced fill factor, we suggest methods of reducing the resistivity and recovering the fill factor. *Published by AIP Publishing*. [http://dx.doi.org/10.1063/1.4967921]

I. INTRODUCTION AND BACKGROUND

In this field of photovoltaics, the open circuit voltage (Voc) is one of the cell's critical properties. The standard Voc is defined as the external voltage which develops across an infinitely high resistance load (hence open circuit) under standard AM1.5G solar illumination. It is known that when the contacts to the solar cell are pinned well into the electronic gap, and a barrier is formed, there is a significant loss of built-in potential which, if undealt with, results in a significant loss of open circuit voltage.[1] In the context of organic materials, Braun *et al.*[2] have argued that effects like that of the integer charge transfer state would induce pinning significantly below (above) the LUMO (HOMO) level. Also, there is some evidence that the built-in potential is currently limiting the performance even if the cells do not possess obviously bad contacts.[3] The most common way to deal with contact's barrier, due to pinning or other factors, would be to introduce blocking contacts or blocking layers[4–6] that are also referred to as single carrier membrane.[7] Unfortunately, practical schemes that follow this concept indicate that, at least for organic cells, the enhancement in open circuit voltage is often associated with loss in the cells fill-factor (FF) such that the overall efficiency does not significantly improve.[8,9] Enhancement of Voc at the expense of the fill factor is also observed in high quality CdTe cells.[10] Recently, an alternative strategy termed the "band gap enhanced structure" was suggested as a way to overcome contacts-related open circuit losses.[11,12] Here, we revisit the blocking-layer method through detailed device simulations. We point to the reason behind most practical implementations having shown an S shape and suggest design rules to overcome it.

We start by describing the numerical model (implemented in Matlab). The results section starts with reintroducing the blocking-layer as a method to enhance V_{oc} and is followed by an analysis of the role of these layers in determining the device performance. The resulting design rules are part of the summary.

II. SIMULATION DETAILS AND PARAMETERS

A. Equations

In this work, we have implemented a numerical calculation that solves simultaneously for the internal electric field and the charge carriers distribution in a given device structure and a given set of physical processes. By device structure, we mean the materials and layers, the interfaces between layers, and the boundary conditions set by the contacts on both ends. Among the physical processes are the photo-generation and recombination processes which may be linked to the mobility and diffusion values. The code is implemented in Matlab, and the numerical solution process follows the Scharfetter & Gummel approximation.[13]

In short, and dealing only with 1-dimentional calculation, the model relates the potential distribution along the device, $\Psi(x)$, to the free electrons and holes distribution, n(x) and p(x) via Poisson equation (1), the continuity equations (2) and (3), and the drift-diffusion current expressions in (6) and (7).

The Poisson equation for the 1D case is

$$\frac{d^2\psi}{dx^2} = \frac{q}{\varepsilon\varepsilon_0}(n-p) \tag{1}$$

with q, ε_0, and ε being the elementary charge unit, vacuum permittivity, and relative permittivity, respectively. The continuity equations relate the change in charge carriers' density to the change in electrical current and to the generation-recombination processes

$$\frac{dJ_n}{dx} - q\frac{dn}{dt} = q(R-G), \tag{2}$$

$$\frac{dJ_p}{dx} + q\frac{dp}{dt} = -q(R-G), \tag{3}$$

a)Author to whom correspondence should be addressed. Electronic mail: nir@ee.technion.ac.il

with J_n (J_p) being the electrical currents in the x-direction (perpendicular to the device surface) for electrons (holes). R and G are recombination and generation rates, respectively. Solving for the steady state, (2) and (3) reduce into

$$\frac{dJ_n}{dx} = q(R - G), \tag{4}$$

$$\frac{dJ_p}{dx} = -q(R - G). \tag{5}$$

Expressing the current as a balance between drift-diffusion currents

$$J_n = qn\mu_n E + qD_n \frac{dn}{dx}, \tag{6}$$

$$J_p = qn\mu_p E - qD_p \frac{dp}{dx} \tag{7}$$

with $\mu_{n,p}$ being the mobility of electrons/holes, $D_{n,p}$ being their diffusion coefficient, and $E = -\frac{d\psi}{dx}$ being the electric field. In this paper, the recombination was taken to be only the Shockley-Reed-Hall (SRH) type,[14–16] in the form

$$R_{SRH} \approx \frac{C_n N_t}{2n_i \cosh\left(\frac{\Delta E_t}{kT}\right)}\left(np - n_i^2\right), \tag{8}$$

with ΔE_t being the trap position relative to the middle of the gap, n_i is the intrinsic charge density (i.e., due to the thermal excitation in the dark), C_n is the trap's capture cross section, N_t is the trap's density, k is the Boltzmann's constant, and T is the temperature. Note that unlike in Refs. 11 and 12, the trapped charges are not explicitly simulated.

B. Boundary conditions

The potential difference between the electrodes has to reflect the external applied voltage. This is implemented such that the potential of the cathode (ψ_1) is set to match its work functions (WFs) and the potential of the anode (ψ_N) equals that of the cathode plus the applied bias. Namely, at zero bias, it equals that of the cathode, and when the applied bias equals the built-in potential (see Figure 1), it equals its own WF. The charge densities at the contacts (n_1, n_N, p_1, and p_N) are determined by the barrier at each electrode ($\Delta E_{cathode/anode}$) following Boltzmann distribution:

$$\begin{cases} n_1 = N_{DOS} \exp\left(-\dfrac{|LUMO - E_{cathode}|}{kT/q}\right) \\ n_N = N_{DOS} \exp\left(-\dfrac{|LUMO - E_{anode}|}{kT/q}\right) \end{cases} \tag{9}$$

$$\begin{cases} p_1 = N_{DOS} \exp\left(-\dfrac{|E_{cathode} - HOMO|}{kT/q}\right) \\ p_N = N_{DOS} \exp\left(-\dfrac{|E_{anode} - HOMO|}{kT/q}\right), \end{cases} \tag{10}$$

with N_{DOS} being the effective density of states, LUMO/HOMO the energy levels of the materials adjacent to the relevant electrode (in eV). Unless stated otherwise, the parameters used in the simulations are shown in Table I.

III. RESULTS AND ANALYSIS

A. The role of charge blocking layers

To reintroduce the effect of blocking layers on solar cells performance, we simulated 3 device structures. The energy levels diagrams of the three solar cells are plotted in Figures 1(a)–1(c). The first (Figure 1(a), device A) is a simple structure with no blocking layer, the second (Figure 1(b), device B) has an additional hole blocking layer (HBL), and the third (Figure 1(c), device C) has both hole- and electron blocking layers (HBL and EBL). Note that Figures 1(a)–1(c) refer to the layers before they are brought into contact; thus, the energy levels are flat. Also, the blocking layers are added such that if the standard device occupies x = 0:160 nm, the HBL occupies negative x values and the EBL is at x > 160 nm. To reinforce the effect of blocking, we have also assumed the mobility of the blocked carrier to be 100 fold lower (see Table I). In all three structures, the contacts have work functions (WF) of 4.4 eV and 4.9 eV below the vacuum level, leading to identical V_{bi} of 0.5 V. Figure 1(g) illustrates the physical processes accounted for the simulation: (1) the device is illuminated from the cathode side. (2) Photons are being absorbed in the active layer and generate free charge carriers (one may refer to the active layer as bulk heterojunction, meaning a volume in which excitons are being excited and dissociated). (3) Free charge carriers are transported to their respective electrodes and contribute to the photocurrent. The charge blocking, which is part of the device structure, is illustrated for a hole that is blocked at the HBL (4). The dotted lines mark Fermi energy levels, being the intrinsic level, in the middle of the electronic gap, before illumination (Figures 1(a)–1(c)), or split into quasi electrons- and holes- Fermi level under illuminations (Figures 1(d)–1(f)).

Figure 1(h) shows J-V curves of the three simulated devices under one sun AM1.5G illumination. In all devices, the active layer thickness is 160 nm and the blocking layers (if exist) are 12 nm wide. For device A (solid blue line), in which the active layer is sandwiched between two contacts, V_{oc} is almost identical to V_{bi}, being 0.5 V. For device B (dashed red line), with additional HBL, V_{oc} exceeds V_{bi} to slightly above 0.6 V. For device C (dotted green line), with both HBL and EBL, V_{oc} is about 0.75 V. While the Voc increases by 50% and the J_{SC} by 10%, the fill factor (FF) is almost unchanged and is ~0.48, leading to PCE increase from 2.6% to 4.4%.

To gain more insight into the blocking process, we present in Figures 1(d)–1(f) the energy levels diagrams of the different devices at open circuit condition (V_{oc} varies between devices). We remind the reader that to arrive at this energy level diagram the model first computes the internal potential, using the Poisson equation, and then adds this potential to the unperturbed levels (Figures 1(a)–1(c)) to result in the energy level diagram under excitation. Figure 1(d) shows that for the standard structure, the bands are flat, but both quasi Fermi levels bend inwards towards

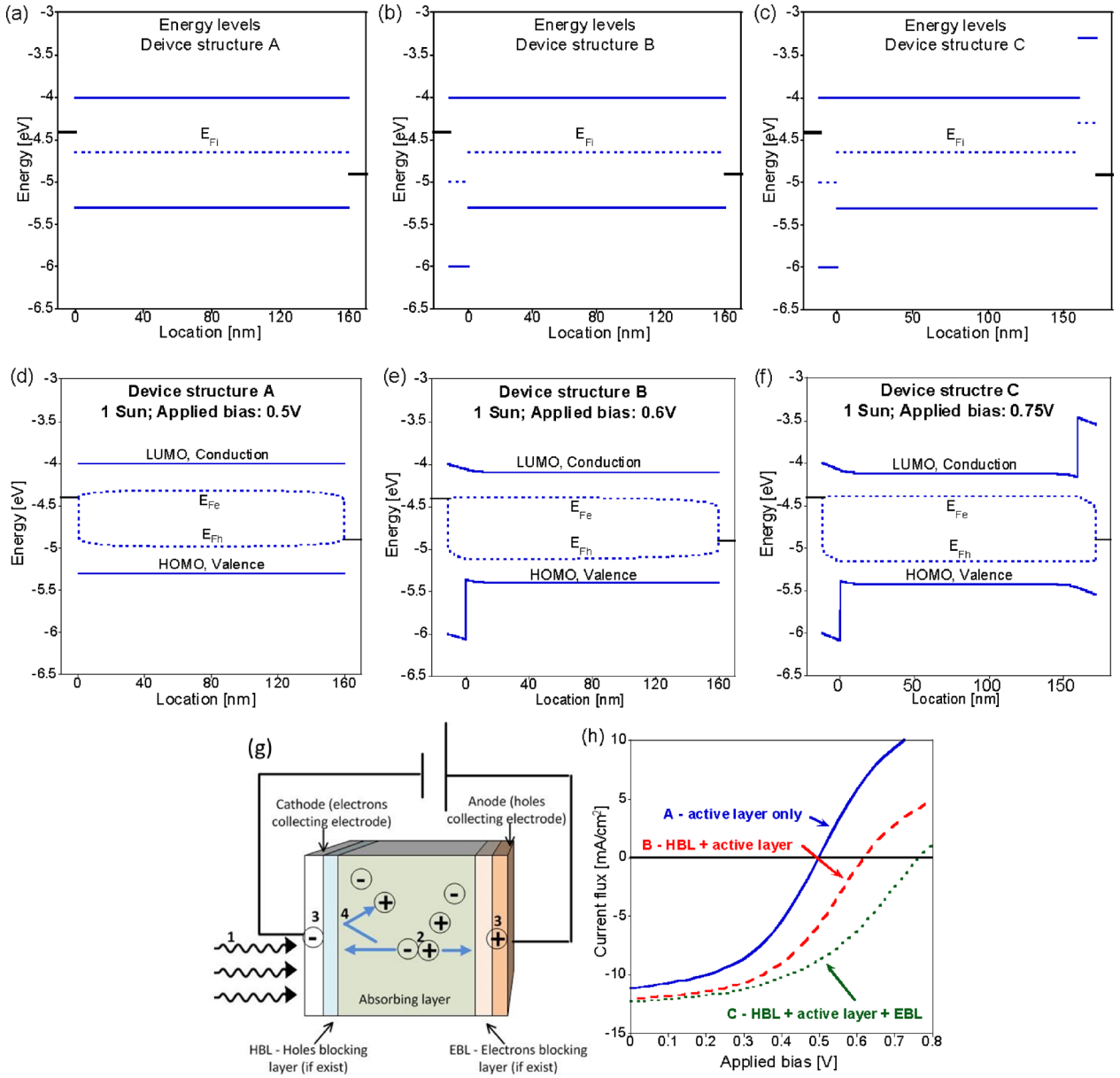

FIG. 1. Energy diagrams of the 3 simulated solar cells, ((a)–(c)) before layers are brought into contact, ((d)–(f)) under applied bias of 0.5/0.65/0.75 V, close to the Voc for each device. ((a) and (d))—Device A, single active layer sandwich between two electrodes. ((b) and (e))—Device B, with additional HBL. ((c) and (e))—Device C, with both HBL and EBL. (g) Schematic diagram of the simulated structure and main physical process (see text). (h) J-V curve, calculated for the three devices under standard AM1.5G sun illumination.

TABLE I. Simulations parameters.

Parameter	HBL (left-hand side)	Active layer	EBL (right-hand side)
LUMO (eV)	4.0	4.0	3.3
HOMO (eV)	6.0	5.3	5.3
ε_0 - relative permittivity	1.46	1.7	1.46
N_{DOS} - density of states (cm^{-3})	10^{21}	10^{21}	10^{21}
μ_n - electron mobility ($cm^2/V/s$)	1×10^{-3}	1×10^{-3}	1×10^{-5}
μ_p - hole mobility ($cm^2/V/s$)	1×10^{-5}	1×10^{-3}	1×10^{-3}
Thickness (nm) unless detailed in the legend	0/12	160	0/12
$C_n N_t (s^{-1})$	3.3×10^5	3.3×10^5	3.3×10^5
$2n_i \cosh\left(\frac{\Delta E_t}{kT}\right) (cm^{-3})$	10^{15}	10^{15}	10^{15}
Metal WF – cathode (eV)	4.4	…	…
Metal WF – anode (eV)	…	…	4.9

the contacts. This is a sign of current flowing towards the contacts due to the contact induced surface recombination (see also discussions in Refs. 11 and 12). In Figure 1(e), a hole blocking layer is introduced, and we note that its energy levels are bent upwards to allow for the open circuit to exceed the built-in potential. The quasi Fermi-level of the holes still bend inwards inside that HBL indicating that there is still some recombination at the contact which induces hole current. However, the quasi Fermi-level of the majority carriers is practically flat, indicating that the contact losses are low enough to be considered negligible. In Figure 1(f), where both HBL and EBL are introduced, one notices an up (down) shift of the LUMO (HOMO) level near the cathode (anode). Again, this is the effect through which the open circuit voltage exceeds V_{bi}. Since the energy difference between the metal WF and the energy levels of the BL is fixed, the increase of the energy separation between the two electrodes has to be accompanied by a bend in the levels. With respect to the open circuit voltage only, the effect of this bend is similar to that of an additional dipole shifting the contact's WF relative to the bulk of the device. Note that the band bending near the contact is such that it opposes the outflow of the generated current. We will refer to this serial resistance effect in Section III B.

To shed more light on the mechanisms affecting the different device characteristics, we present in Figure 2 the distribution of both free electrons (Figure 2(a)) and holes (Figure 2(b)) in the three simulated devices (Figures 1(a)–1(c)). The bias applied to all the devices is 0.5 V which is exactly the WF difference between the electrodes (thus equals V_{bi}), and the devices are simulated under one sun illumination. The vertical dashed lines mark the active layer to which BL might be added. In device A, without any blocking layers, the distribution is symmetric and is very similar between electrons and holes. This is despite the a-symmetry of the generation process (following the Beer-Lambert law, with light hitting the device through the cathode). Also, noticeable is the distributions peak at the center of the active layer, dropping towards the electrodes. Just like the inward bend of the quasi-Fermi levels, the carrier densities' drops indicate the "sink" characteristic of the contacts, in which recombination takes place and reduces the amount of charge carriers within the device. The distribution shape and its symmetry indicate that the contact-recombination is dominant which is to be expected for a device where the electrodes are pinned well into the gap. In device B, with the introduction of HBL between the cathode and the active layer, there are practically no holes in the blocking layer, and the holes' density at the HBL/active layer interface is raised to above $2.5 \times 10^{16}\,cm^{-3}$ (Figure 2(b), red dashed line). Eliminating the recombination at the cathode interface has two major effects: First, it reduces the overall recombination; thus, the overall charge density increases. Second, it introduces asymmetry in the losses as the recombination at the anode interface is still active. Introducing the EBL as well eliminated the recombination at the anode interface, thus making the recombination profile more symmetric. The asymmetry seen for both holes and electrons distribution (Figure 2, green dotted line) is due to the asymmetry of the excitation profile as the absorption is assumed to follow an exponential decay with an absorption depth of 150 nm and the illumination through the cathode (left) side.

B. The blocking layers' resistance

In Section III A, we found that adding the blocking layers reduces, or eliminates, the contacts' recombination and allows the open circuit voltage to exceed the energy difference between the contacts' work functions. It was shown that the increase in V_{oc} is due to band bending of the BLs and that the effect on V_{oc} is similar to that of dipoles that shift the bands. The simulations also showed that the fill factor was almost not affected which follows the basic theory,[17] but for most practical cases, one observes a severe S shape and a reduced fill factor.[8,9] Below, we try to provide an explanation for the observed loss of fill factor.

1. Layers' mobility

As the title of this section implies, it is the resistivity of the BLs that is probably responsible for the appearance of an S shape. As the effect of a given resistivity is always dependent on its value relative to other factors, we present in Figure 3(a) the J-V as a function of the active layer thickness while keeping the BLs thickness at 12 nm. The first effect of enhancing the active layer thickness from 40 nm to 200 nm is that more light is absorbed and the short circuit current

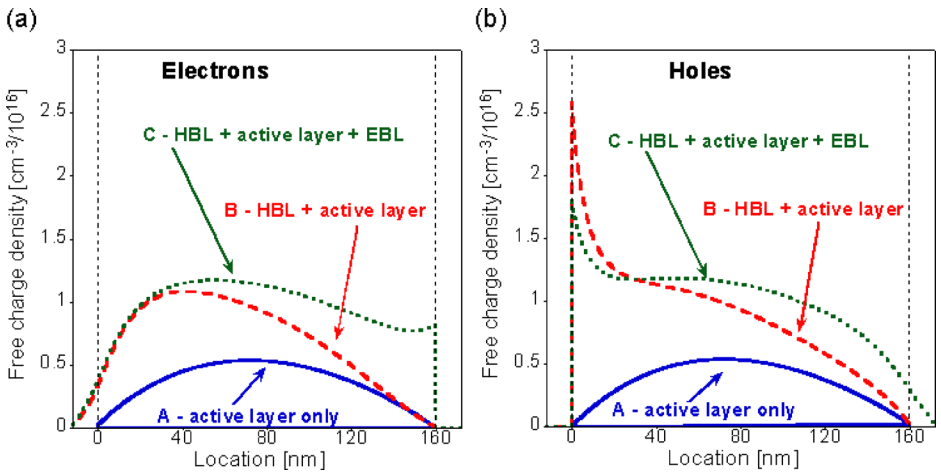

FIG. 2. Charge carriers' density distribution of electrons (a) and holes (b) in the three simulated devices (see Figures 1(a)–1(c)). The applied bias is 0.5 V, and the illumination is one sun (through the cathode side). See main text for the effects governing these distributions.

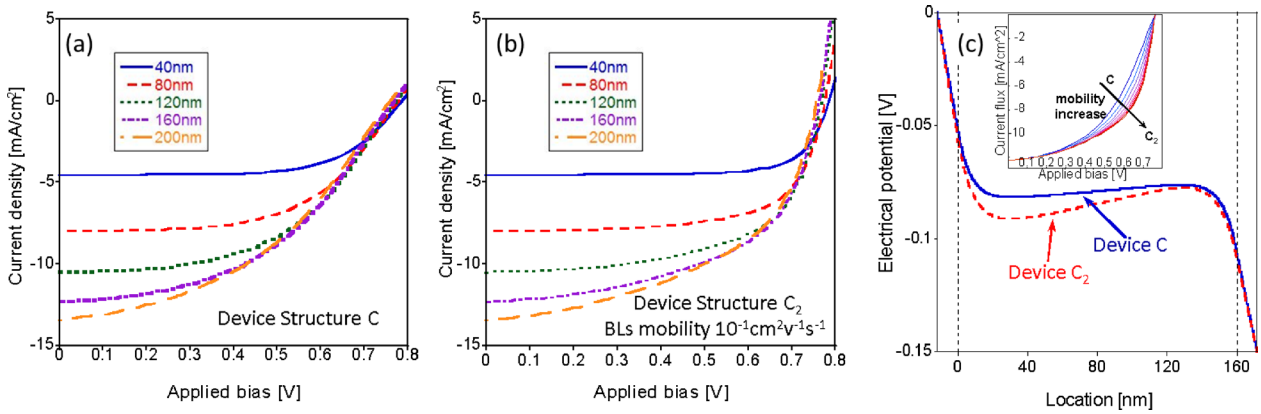

FIG. 3. (a) J-V curves of devices of type C, with varying active layer thickness (see legend). (b) same as in (a) but for 100 fold higher mobility value at the BLs. (c) Electrical potential in one representative of C and one representative of C_2 (both with 160 nm active layer), at applied bias of 0.65 V. The cathode is arbitrary set as V = 0. Inset: J-V curve while gradually changing the mobility value at the BLs from C to C_2.

increases. The other effect is that with the increase in the short-circuit current, the S shape becomes more apparent as more voltage drops across the BLs' serial resistance. To corroborate that the effect has to do with the blocking layers' resistivity, we repeated the simulations but now assumed that the mobility, of the relevant charge carrier, in the BL is enhanced by two orders of magnitude (10^{-1} instead of 10^{-3} $cm^2\ v^{-1}\ s^{-1}$). We term this device structure, with enhanced mobility at the BLs, as C_2. Figure 3(b) shows the results of these simulations, and we indeed see that the S shape has completely disappeared and that the fill factor has increased. To place in perspective the device performance of the various device structures, we collated their parameters in Table II. We note that adding BLs gradually increases the cells' efficiency and that making the mobility at the BLs higher by a factor of 100 makes an additional significant contribution to the cells' efficiency.

Figure 3(c) shows the internal electric potential of 160 nm active layer devices of both uniform mobility ($10^{-3}\ cm^2\ v^{-1}\ s^{-1}$ in all layers) and enhanced mobility ($10^{-1}\ cm^2\ v^{-1}\ s^{-1}$) at the BLs. As discussed in the context of Figure 1, this internal potential is what bends the levels. The main feature of this graph is that the band is tilted upwards at the cathode side and downward at the anode side. This effectively opens the energy gap between the contacts work functions to enable higher V_{oc}. On the other hand, the direction of the slope is such that it resists the exit of electrons on the left (cathode) and holes on the right (anode). This is actually the source of the added resistance that can be minimized by making the charge mobility much higher. The other feature is the slope of the band in the bulk of the device. We note that when the resistivity of the BLs is minimized, the slope of the bands is higher, thus further enhancing photocurrent extraction and improving the fill factor.

2. Layers' thickness

While in Section III B 1 we discussed the fact that practical BLs exhibit finite carrier mobility, here we examine their finite thickness. As it is difficult to fabricate a 10 nm thick film with no pin-holes, and as evaporated metals can induce transport states or dope such thin layers, one may tend to use thicker layers. We again use device structure C with both EBL and HBL, but now, we vary the BL's thickness while keeping the active layer thickness fixed at 160 nm. As before, the devices with enhanced carrier mobility in the BLs will be termed C_2. Figure 4(a) presents J-V curves of devices of type C for blocking layer thickness between 5 and 50 nm. We note that already at 25 nm, there is a significant degradation in device performance that is more pronounced in the 50 nm case. In accordance with Section III B 1, to ensure that the reduced performance is indeed associated with the BLs resistivity, we repeated the simulation but assumed that the relevant carrier mobility at the BL is 100 fold higher. Figure 4(b) shows that, indeed, for high mobility BLs all curves merge and are at the best value one can expect from the active layers properties.

Similar to Figure 3(c), we plot in Figure 4(c) the electrical potential distribution under applied bias of 0.65 V but for 50 nm thick blocking layers. Relative to Figure 3(c), the effects here are more pronounced for the structure without the enhanced mobility (Figure 4(a)), as the serial resistance introduced by the 50 nm BLs is significant.

TABLE II. Properties of the various simulated solar cell structures having active layer thickness of 160 nm.

Device	BLs	J-V figures	J_{cs} (mA/cm^2)	V_{oc} (V)	FF (%)	PCE (%)
A (Figure 1(a))	None	Figure 1(h) solid blue	11.1	0.50	47	2.6
B (Figure 1(b))	HBL	Figure 1(h) dashed red	12.0	0.61	49	3.6
C (Figure 1(c))	HBL + EBL	Figure 1(h) dotted green	12.3	0.76	47	4.4
		Figure 3(a) purple dashed-dotted				
C_2 (Figure 1(c))	HBL + EBL improved μ	Figure 3(b) purple dashed-dotted	12.3	0.76	55	5.2

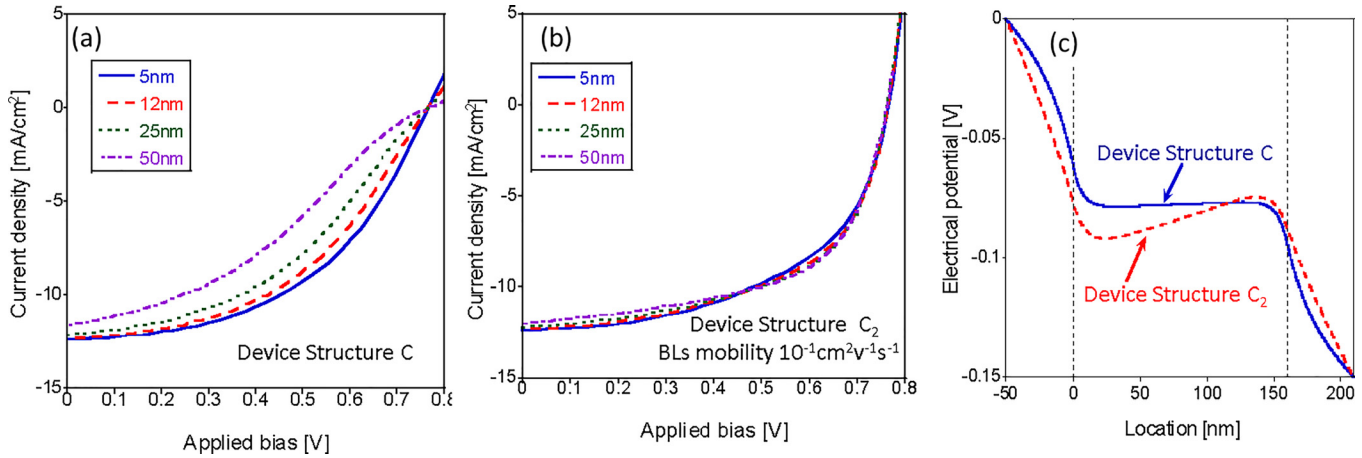

FIG. 4. (a) J-V curves of devices of type C, with varying blocking layer thickness (see legend). (b) same as in (a) but for 100 fold higher mobility value at the BLs. (c) Electrical potential in one representative of C and one representative of C_2 (both with 50 nm blocking layer in each side), under applied bias of 0.65 V. The cathode is arbitrary set as V = 0.

IV. SUMMARY AND DISCUSSION

Before summarizing the results above, and as pointed out by the anonymous referee, the paper would not be complete without some general discussion of the S shape phenomenon. To do so, we show in Figure 5(a) an illustration showing the general features of an S shape in the I–V curve. Next, we make a simplifying assumption that below V_{OC} all the measured current is photocurrent, and we change the variables used to present Figure 5(a). In Figure 5(b), the x axis is the internal potential which is the built-in potential minus the applied voltage and the y-axis is the photocurrent.

Examining Figure 5(b), we see that the part of the S shape that interests us looks like a diode response. In fact, more generally, it exhibits a current that is voltage dependent. In this case, it means that the current depends on the internal potential or the internal electric field. Staying with the general and simple picture, we can write the balance of processes, Equation (11), as a balance between photo-carrier generation (G), extracted current (J), and photo-carrier recombination (R)

$$G_{eneration}(V_{\text{int}}) = J_{extracted}(V_{\text{int}}) + R_{ecombination}(V_{\text{int}}). \quad (11)$$

In the most general case, any of the processes noted in Equation (11) could introduce a dependence on the internal potential (V_{int}). In excitonic semiconductors, it is known that the separation of the exciton into free carriers could be field dependent as in the Onsager-Braun theory.[18] Recombination dependence on the internal field is often mentioned in the context of geminate recombination which could also be regarded as a reduction in the generation of free charges. However, while the free charge carrier recombination may not be directly dependent on the internal field (E_{int}), it may present internal-potential dependence due to the super-linear dependence on the charge density which, in turn, depends on the internal bias.[19] The last, but not least, is the extracted current where for bias levels up to few kT below the open circuit voltage it can be regarded as a purely drift current: $J_{extracted} = \mu E_{\text{int}} n$. The real question regarding the current is whether it is limited by the generation-recombination balance or by the ability of the charges to exit the device. This is somewhat similar to the bulk-limited and injection limited regimes in light emitting diodes. The major difference is that the equivalent of injection in solar cell is (G-R), and hence, a good solar cell is "injection" limited. One of the factors that may affect the extraction, and make the photo-current limited by something different than (G-R), is the mobility value being very low such that a large enough internal field is required to make sure charges can drift to the contacts within their recombination lifetime. The other factor is the contact or the contact region which may constitute a barrier or resistance to charge extraction. From all the mechanisms discussed above, this paper deals only with the last one and the way it may depend on the properties of blocking layers.

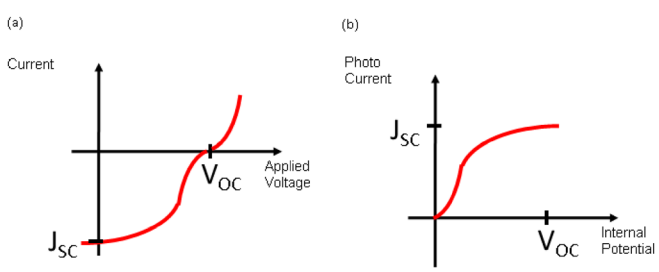

FIG. 5. (a) Illustration of an S shape in the I–V curve of a solar cell under one sun illumination. (b) The same as in (a) but presented as photo-current and as a function of internal potential.

We have used a drift-diffusion-Poisson computational model to rigorously investigate charge blocking layers (BLs) in thin-film solar cells, one specific implementation of "interfacial layers." Both EBLs and HBLs were examined. We were motivated by the argument that cells with V_{oc} that is above V_{bi} are prone to low fill factors or S shape[8,9] although the notion of blocking contacts does not necessarily implies that.[17] We found that when the contact is made a blocking one and the open circuit exceeds the built-in potential, the extra potential or the difference

between V_{oc} and V_{bi} drops across the interface (layer) next to the contact. The slope of these potential drops, at both the anode and cathode side, is such that they oppose charge extraction. This could be viewed as extraction barrier or serial resistance. Namely, the serial resistance and the accompanying S shape are indeed inherent to most practical blocking layers.

We also found that it is possible to design the blocking layers such that the resistivity is minimized and the S shape would disappear, making the blocking as in the ideal blocking contacts. We discussed two obvious, yet challenging, paths to achieve this. First, we use sub 10 nm thick blocking layers. This is challenging because it is very difficult to produce such a thin layer that would truly block charge motion through it. This would be typically due to pinholes and defect assisted tunneling. Second, one could use for the BLs materials with relatively high charge carrier mobility. These are in fact the two attributes used in Ref. 6 where the blocking layers took the ideal role. Manifesting such material properties will require dedicated synthesis aimed at providing not only the right energetic position of the levels but also to result in mobility values of $\sim 10^{-1}$ cm^2 v^{-1} s^{-1}. A third method to reduce the resistivity could be N or P doping of the HBL and EBL, respectively. Such doping may compromise[4] the sought enhanced Voc and is the topic of our future studies.

This dedicated blocking layer design has the potential of recovering loss of open circuit voltage without sacrificing the fill factor providing performance similar to that of the band gap enhanced solar cell structure.[11,12]

ACKNOWLEDGMENTS

This research was carried in the framework of the Grand Technion Energy Program (GTEP) and supported by the Adelis Foundation for renewable energy research.

[1]N. K. Elumalai and A. Uddin, Energy Environ. Sci. **9**, 391 (2016).
[2]S. Braun, W. R. Salaneck, and M. Fahlman, Adv. Mater. **21**, 1450 (2009).
[3]B. Liu, R. Q. Png, J. K. Tan, and P. K. H. Ho, Adv. Energy Mater. **4**, 1200972 (2014).
[4]W. Tress, K. Leo, and M. Riede, Phys. Rev. B **85**, 155201 (2012).
[5]E. L. Ratcliff, B. Zacher, and N. R. Armstrong, J. Phys. Chem. Lett. **2**, 1337 (2011).
[6]U. Wurfel, D. Neher, A. Spies, and S. Albrecht, Nat. Commun. **6**, 6951 (2015).
[7]P. Wurfel, *Physics of Solar Cells* (Wiley-VCH Verlag GmbH, Weinheim, Germany, 2005).
[8]W. Tress and O. Inganäs, Sol. Energy Mater. Sol. Cells **117**, 599 (2013).
[9]T. Kirchartz, W. Gong, S. A. Hawks, T. Agostinelli, R. C. I. MacKenzie, Y. Yang, and J. Nelson, J. Phys. Chem. C **116**, 7672 (2012).
[10]J. M. Burst, J. N. Duenow, D. S. Albin, E. Colegrove, M. O. Reese, J. A. Aguiar, C.-S. Jiang, M. K. Patel, M. M. Al-Jassim, D. Kuciauskas, S. Swain, T. Ablekim, K. G. Lynn, and W. K. Metzger, Nat. Energy **1**, 16015 (2016).
[11]N. Tessler, J. Appl. Phys. **118**, 215501 (2015).
[12]N. Tessler, Appl. Phys. Lett. **108**, 183503 (2016).
[13]S. Selberherr, *Analysis and Simulation of Semiconductor Devices* (Springer-Verlag, Vien, 1984).
[14]L. Tzabari, V. Zayats, and N. Tessler, J. Appl. Phys. **114**, 154514 (2013).
[15]L. Tzabari, J. Wang, Y.-J. Lee, J. W. P. Hsu, and N. Tessler, J. Phys. Chem. C **118**, 27681 (2014).
[16]R. A. Street, A. Krakaris, and S. R. Cowan, Adv. Funct. Mater. **22**, 4608 (2012).
[17]P. Würfel and U. Würfel, *Physics of Solar Cells: From Basic Principles to Advanced Concepts* (Wiley-VCH, 2009).
[18]C. L. Braun, J. Chem. Phys. **80**, 4157 (1984).
[19]C. G. Shuttle, B. O'Regan, A. M. Ballantyne, J. Nelson, D. D. C. Bradley, J. de Mello, and J. R. Durrant, Appl. Phys. Lett. **92**, 93311 (2008).